Bull Volcanol (2014) 76:805
DOI 10.1007/s00445-014-0805-y

RESEARCH ARTICLE

Stable chlorine isotope behavior during volcanic degassing of H_2O and CO_2 at Mono Craters, CA

Jaime D. Barnes · Timothy J. Prather · Miguel Cisneros · Kenneth Befus · James E. Gardner · Toti E. Larson

Received: 1 November 2013 / Accepted: 1 February 2014 / Published online: 19 February 2014

Abstract Trends in CO_2 and H_2O concentrations and δD values of obsidian clasts from Mono Craters volcanic field, California demonstrate clear chemical and isotopic evidence for eruptive degassing. However, neither Cl concentrations nor stable isotopes (^{35}Cl and ^{37}Cl) track the degassing process, which is likely because of disequilibrium due to slow diffusion of Cl in the cooling melt. Obsidian pyroclasts (n=29) were collected from tuff layers representing a single eruptive sequence that occurred circa 1340 A.D., as well as, rhyolitic obsidian samples (n=12) were collected from three high-silica (>74 % SiO_2) flows forming the domes and coulees in the region. The Cl, H_2O, and CO_2 concentrations recorded by the eruptive pyroclastic obsidians track the chemical evolution of the magmatic system during eruption, whereas the concentrations of the dome samples represent the final degassed product. The H_2O and CO_2 concentrations of the pyroclastic samples range from 0.49 to 2.13 wt% and 2 to 35 ppm, respectively; whereas concentrations in the dome glasses range from 0.17 to 0.33 wt% and 1 to 3 ppm, respectively. H_2O and CO_2 concentrations in the pyroclastic fall and dome samples are strongly correlated and reflect the degassing trend of the eruptive sequence. Chlorine concentrations of the pyroclastic fall samples and the domes range from 609 to 833 ppm and 681 to 872 ppm, respectively. Cl concentrations do not display a strong correlation with either H_2O or CO_2 concentrations. δD values of the pyroclastic fall obsidians vary between −84‰ and −55‰, whereas the δD values of the dome obsidians vary between −117‰ and −91‰. D/H ratios decrease with total water content following a distillation trend controlled by both closed and open system degassing. $\delta^{37}Cl$ values of pyroclastic fall obsidians (−1.9‰ to −0.1‰) overlap with those of dome samples (−1.2‰ to 0.0‰). The similar Cl concentrations between the pyroclastic fall and dome obsidians argue for lack of Cl degassing, despite H_2O and CO_2 loss. These observations can be explained by disequilibrium effects due to the slow diffusion rate of Cl compared to H_2O and CO_2 in silicate melt, buffering by a separate brine phase, or by fluxing of Cl from a deeper magma source, with the slow diffusion rate of Cl being the preferred explanation. The wide range in $\delta^{37}Cl$ values may be indicative of isotopic compositional heterogeneities in the magma source due to assimilation of sedimentary material or fluxing of mantle-derived Cl to a crustal melt.

Keywords Degassing · Mono Craters · Obsidian · Stable isotopes · Chlorine · Volatiles

Editorial responsibility: M. Manga

Electronic supplementary material The online version of this article (doi:10.1007/s00445-014-0805-y) contains supplementary material, which is available to authorized users.

J. D. Barnes (✉) · T. J. Prather · M. Cisneros · K. Befus · J. E. Gardner · T. E. Larson
Department of Geological Sciences, University of Texas, Austin, TX 78712, USA
e-mail: jdbarnes@jsg.utexas.edu

Introduction

Fluids play a critical role in subduction zones, acting as the primary agents of hydration and serpentinization of the mantle wedge, altering the state of stress at depth, and generating melts that feed volcanic arc systems. Chlorine stable isotopes have been used as a geochemical tracer of fluid sources in subduction zone volcanoes (Barnes et al. 2008, 2009; Barnes and Straub 2010; Rizzo et al. 2013), because of the high solubility of chlorine in aqueous phases and the assumption of little to no fractionation of chlorine stable isotopes (^{37}Cl and ^{35}Cl) at high temperatures. This assumption is based on calculations that predict minimal fractionation between minerals, melt, and fluid at high temperatures (Schauble et al. 2003),

and on limited experimental data between coexisting vapor and liquid in the H_2O–NaCl system (Liebscher et al. 2006). In addition, work on lavas/ejecta from Mt. Etna, Italy, shows 30–70 % Cl loss, based on Cl concentrations in the bulk rock compared to Cl concentrations in melt inclusions, but no correlation between $\delta^{37}Cl$ values and percent Cl loss, implying no fractionation of Cl isotopes during volcanic degassing (Rizzo et al. 2013). However, these data from Mt. Etna are limited to a small sample set ($n=7$). In contrast, recent work has shown that near-surface kinetic fractionation of Cl stable isotopes affects high-temperature (>100 °C) fumarole gases (Sharp et al. 2010). Furthermore, diffusion-controlled isotopic fractionation in silicate melts is generally quite large, even at temperatures approaching 1,450 °C (Watkins et al. 2011). Additional work is thus necessary to assess whether chlorine stable isotopes fractionate during volcanic degassing and progressive volatile loss.

A way to examine possible Cl isotope fractionation during volcanic degassing is an empirical study focusing on a suite of natural pyroclastic materials that underwent variable amounts of degassing. During the process of volcanic degassing, volatiles dissolved in the magma are either released as gases or are trapped in rapidly quenched glasses. Because these glasses represent quenched portions of erupting liquid, they preserve a record of the bulk, trace, and isotopic geochemistry of the magma. Pyroclastic eruptions generate stratigraphic sequences of erupted products, which record the history of the eruptive event. These deposits may contain obsidian pyroclasts, which are thought to be small pieces of the magma that were quenched along the walls of the eruption conduit and then plucked from the walls (e.g., Newman et al. 1988). Because these glasses contain various amounts of dissolved gases, they are assumed to be plucked from various depths, and thus record the volatile evolution of the melt throughout the progression of the eruption. Analyses of the Cl concentration and chlorine isotope composition in these obsidian pyroclasts (coupled with H_2O and CO_2 concentrations and δD values) may provide insight into the behavior of ^{37}Cl and ^{35}Cl during volcanic degassing and allow assessment of the validity in using chlorine stable isotopes as a tracer of source in volcanic systems.

For this study, we selected a suite of obsidian pyroclasts from the well-studied A.D. 1340 eruption and extrusion of the rhyolitic domes in the Mono Craters field, California. Extensive previous work on volcanic degassing has focused on the A.D. 1340 Mono Craters eruption (Newman et al. 1988; Bursik 1993; Rust et al. 2004; Gonnermann and Manga 2005; Watkins et al. 2012). A landmark study by Newman et al. (1988) showed a correlation between H_2O concentrations, CO_2 concentrations, and δD values of pyroclastic obsidians. These co-variations could be explained by a relatively simple two-stage degassing model in which (a) the obsidian pyroclasts produced during the sub-Plinian-style eruption experienced closed-system degassing (i.e., the vapor was not removed from the system, but rather remained in equilibrium with the residual liquid), followed by (b) open-system Rayleigh fractionation (i.e., the exsolved vapor is continuously removed from the system) during the emplacement of the rhyolitic domes (Newman et al. 1988). This model requires the existence of bubbles to accommodate the loss of volatiles from the melt in the closed system, yet the obsidians pyroclasts are generally bubble-free (Newman et al. 1988). Rust et al. (2004) proposed an open-system process, in which the volatile contents are buffered by continuous fluxing of a CO_2-rich vapor from below during shear-induced magma brecciation along conduit walls. Both of these models require a high CO_2 concentration in the parental magma to explain the CO_2/H_2O concentration ratios (Newman et al. 1988; Rust et al. 2004; Gonnermann and Manga 2005). In contrast, Gonnermann and Manga (2005) propose a third model of nonequilibrium, closed-system and permeability-controlled open-system degassing to explain the H_2O and CO_2 concentration trends, thus removing the requirement of a CO_2-rich vapor buffer and high bubble density. H_2O and CO_2 concentration gradients near bubbles in obsidian pyroclasts support nonequilibrium degassing during the Mono Craters eruption, although do not exclude the possible presence of a CO_2-rich vapor (Watkins et al. 2012). The goal of this study is not to resolve these issues, but rather, to investigate the behavior of chlorine. The degassing (or regassing) models described above provide a framework in which to interpret the behavior of chlorine in a well-characterized and well-studied system.

Geologic setting and sampling

The Mono craters region delineates the western perimeter of the Basin and Range province of North America, bounded to the east by the eastern central Sierra Nevada, to the south by the Long Valley Caldera, and to the north by the Bodie Hills (Sieh and Bursik 1986; Bursik and Sieh 1989). This region experienced widespread volcanism in the late Quaternary, associated with dike intrusions related to range-front normal faulting that is characteristic of Basin and Range extension (Bursik and Sieh 1989). Effusive and explosive rhyolitic volcanism during the late Pleistocene began approximately 40,000 years B.P., producing a north–south trending chain of silicic domes, and substantial pyroclastic deposits typical of sub-Plinian to Plinian eruptions. All the lavas within the Mono craters are relatively homogeneous, high-silica rhyolites (~74–77 wt% SiO_2), with the exception of one rhyodacite (Wood 1983; Kelleher and Cameron 1990). The high-silica rhyolites are aphyric to slightly porphyritic, with ~3–8 volume % phenocrysts of sanidine, plagioclase, and quartz, and minor amounts of biotite, hornblende, orthopyroxene, fayalite, and various accessory phases (magnetite, zircon, apatite, allanite;

Wood 1983; Kelleher and Cameron 1990). However, there is some variability in trace-element geochemistry, particularly within the biotite-bearing domes, implying a different chemical evolution from the other high-silica rhyolites (Kelleher and Cameron 1990).

The circa 1340 A.D. eruption of vents in the northern and central portion of the Mono Craters region produced pyroclastic fall deposits over the time span of a few months, followed by pyroclastic flows and surge deposits, and finally emplacement of five rhyolitic domes and coulees within a few years, starting at North Coulee and trending northward to Panum Crater (Wood 1983; Sieh and Bursik 1986; Fig. 1). The ~1340 A.D. eruption is nearly coeval with the latest eruption of the Inyo volcanic chain, ~20 km to the south, but recent geochemical work precludes linking the two eruptions to a common magma source (Higgins and Meilleur 2009).

Obsidian clasts for this study were collected from a ~1.5-m-deep pit dug into conformable pyroclastic fall deposits to the east of Panum Crater Dome (Figs. 1 and 2). Clasts, approximately 1–2 cm in diameter, were picked from two stratigraphic horizons: a lower layer (named P2) and an upper layer (named P10; Fig. 2). Layer P2 is a lithic-rich, pumice fall, and layer P10 is a coarse, lithic-rich, normally graded pumice fall. Obsidian dome samples were also collected from three of the five rhyolitic domes (Panum Crater Dome, Northwest Coulee and North Coulee; Fig. 1). In addition, S. Newman provided three samples from the Newman et al. (1988) study: a chip from a large airfall obsidian block from south of North Coulee (Mc84df-lt), a chip from a Panum dome block-and-ash flow (Mc84-t), and one dome obsidian sample from North Coulee (N Coulee).

Obsidians from layer P2 are essentially holohyaline (entirely glassy) with trace amounts (<<~0.1 %) of pyroxene and FeTi oxide microlites. Obsidian pyroclasts from layer P10 are also nearly holohyaline with slightly more microlites (~0.5 %), consisting primarily of FeTi oxides and lesser amounts of pyroxene and feldspar. No hydrous phenocryst or microlite phases were observed in obsidians from either P2 or P10. The large obsidian block (Mc84df-lt) contains ~1 % microlites, consisting of pyroxene, feldspar, oxide minerals, and rare greenish-brown biotite. All of the dome samples, including the Panum flow (Mc84-t), contain ~2–5 % microlites of pyroxene, oxide minerals, and feldspar. Very rare, reddish-brown biotite microlites are observed in North Coulee.

Analytical methods

H_2O, CO_2, and Cl concentrations

Each obsidian chip and obsidian dome sample was broken apart and fragments, approximately 3 mm in diameter, were

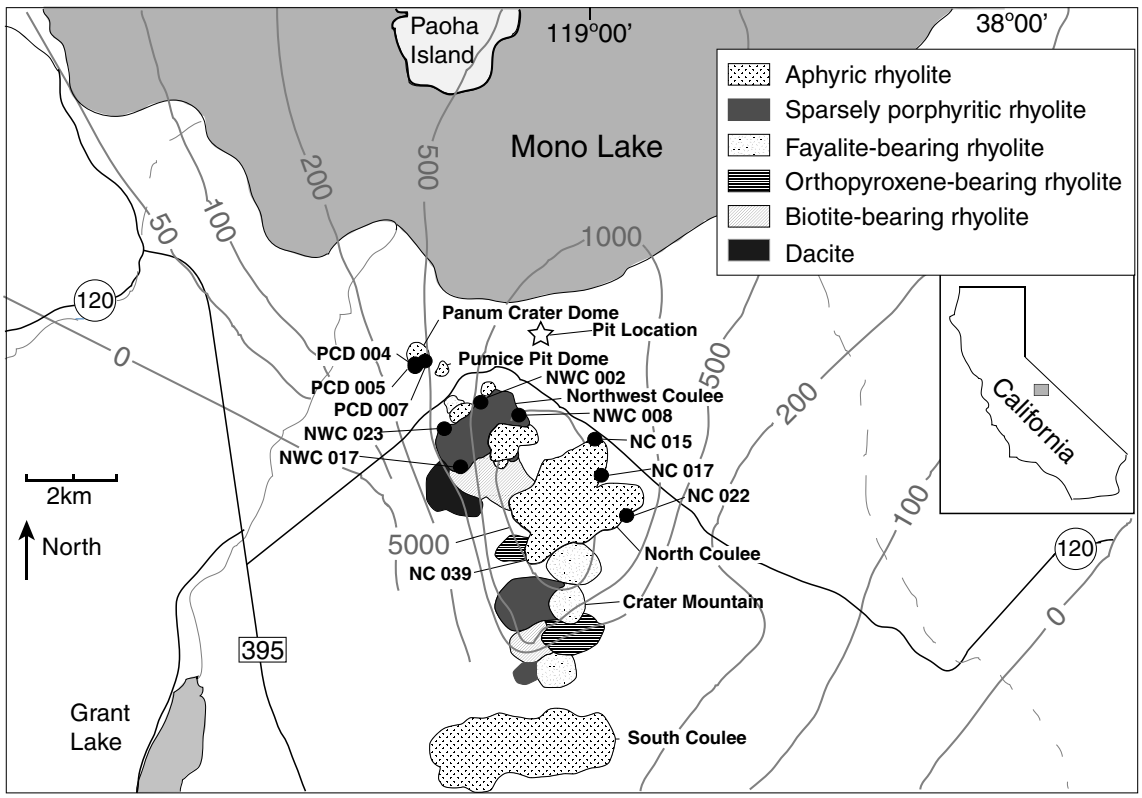

Fig. 1 Map of the Mono Craters region (modified after Newman et al. 1988 and Kelleher and Cameron 1990). *Contours* are isopachs in feet for the total airfall from the 1340 A.D. eruptions. *Star* shows the location of the trenched pit (Fig. 2), and *black circles* show the location of dome samples

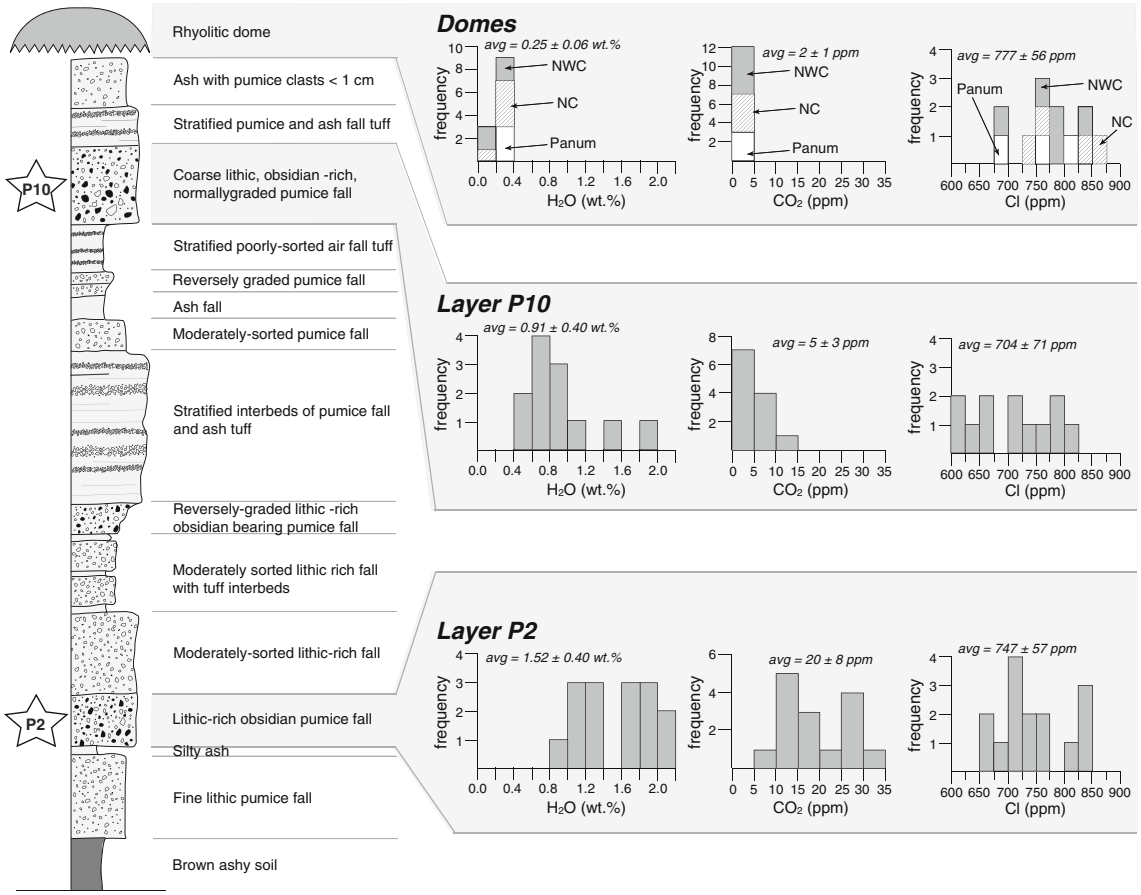

Fig. 2 Schematic stratigraphic section of the 1.5-m deep pit trenched near Panum Crater Dome; layers P2 and P10 are highlighted with *stars*. Histograms show the frequency and range of H_2O, CO_2, and Cl concentrations of obsidians from P2, P10, and the domes. Data from Panum Crater (Panum; *white*), North Coulee (NC; *stripes*), and NWC (Northwest Coulee; *dark gray*) are distinguished

taken from the center to avoid surficial contamination and hydrated rind material. Each fragment was mounted in resin epoxy, and doubly polished for Fourier Transform Infrared Spectroscopy (FTIR) analysis, utilizing the Thermo Electron Nicolet 6700 FTIR spectrometer and Continuum IR microscope at the University of Texas at Austin. These doubly polished wafers of the clasts were then analyzed for dissolved water and carbon dioxide contents at three spots per clast, with care taken to avoid vesicles, microlites, and/or surface impurities.

Each spectrum consisted of 60 scans collected at a resolution of 4 cm^{-1}. Spectra were collected in both mid-IR, using a KBr beam-splitter and globular IR source, and in near-IR, using a CaF_2 beam-splitter and white light. Total water concentrations of the obsidian pyroclasts were estimated from absorbances at about 5,230 and 4,500 cm^{-1} resulting from molecular water (H_2O_m) and bound hydroxyl (OH; Ihinger et al. 1994). Concentrations of H_2O_m and OH were calculated from absorbances using the model of Zhang et al. (1997). The sum of concentrations of the two water species is termed H_2O_{total}. Total water concentrations of the dome obsidians were estimated using absorbance at ~3,500 cm^{-1} (H_2O_{3500}). Concentrations of dissolved molecular carbon dioxide (CO_2) were determined from absorbance at 2,350 cm^{-1}. We assumed linear backgrounds for absorbances at 5,230, 3,500, and 2,350 cm^{-1}. Background for absorbance at 4,500 cm^{-1} was estimated using a French curve set tangential to the IR spectrum on either side of the peak. The concentrations of dissolved H_2O_{3500} and CO_2 were calculated using a modified Beer–Lambert law. We used a value of 1,214±16 L/(cm·mol) for the molar absorptivity of CO_2 (Behrens et al. 2004) and a value of 70 for the molar absorptivity of H_2O_{3500}, which is similar to published values appropriate for the ranges in water content and speciation in our samples (Newman et al. 1986; Dobson et al. 1989; Ihinger et al. 1994; Behrens and Schmidt 1998; Okumura et al. 2003; Leschik et al. 2004; Befus et al. 2012).

Glass density was assumed to be 2,355 g/L and was not adjusted for water content. Thickness (d) was measured using a linear decoder and a petrographic microscope. The calculated values for water and carbon dioxide concentrations were then averaged for each clast and reported in weight % and ppm, respectively (Table 1). Errors (1σ) listed in Table 1 are based on the average of the three individual spot analyses of

Table 1 Average total H_2O, CO_2, and Cl concentrations and δD and $\delta^{37}Cl$ values of Mono Crater obsidians

Sample	H_2O_{total} (wt.%)[a]	1σ (H_2O_{total})	CO_2 (ppm)	1σ (CO_2)	Cl (ppm)	δD (‰)	$\delta^{37}Cl$ (‰)
Layer P2							
P2-A	1.11	0.03	17	3	827	−67	−0.6
P2-B	1.75	0.01	14	7	716	−59	−0.1
P2-C	1.64	0.07	19	2	702	−55	−0.8
P2-D	1.21	0.07	13	1	674	−69	−1.9
P2-H	1.10	0.08	15	4	679	−68	−0.4
P2-I	1.91	0.15	35	15	826	−61	−0.9
P2-J	0.91	0.02	8	0	748	−71	n.d.
P2-K	1.35	0.03	13	1	675	−66	−0.3
P2-M	1.89	0.07	29	7	819	−72	−1.1
P2-N	1.88	0.12	26	2	766	−62	−0.4
P2-O	1.25	0.25	14	4	722	−72	−0.2
P2-P	1.08	0.09	20	2	723	−67	−0.7
P2-Q	2.02	0.12	26	0	833	−64	−1.8
P2-S	1.62	0.06	21	1	734	−66	−1.3
P2-T	2.13	0.14	29	1	757	−66	−0.1
Layer P10							
P10-A	1.60	0.36	6	2	735	−67	−1.3
P10-B	1.80	0.09	13	2	780	−62	−0.4
P10-C	0.84	0.06	2	1	711	−79	−0.7
P10-D	0.94	0.21	2	1	656	−76	−1.0
P10-E	0.67	0.09	3	0	756	−76	−1.0
P10-F	0.71	0.05	5	1	808	−84	−0.7
P10-G	0.83	0.03	5	0	632	−76	−1.5
P10-H	1.06	0.10	5	2	711	−71	−0.5
P10-I	0.49	0.04	6	3	609	−79	−1.4
P10-J	0.78	0.06	5	0	654	−76	−0.1
P10-K	0.56	0.01	5	1	788	−80	−0.6
P10-M	0.65	0.07	3	1	609	−82	−0.7
Rhyolite domes							
PCD-004	0.26	0.01	1	1	699	−100	−0.8
PCD-005	0.31	0.02	2	2	816	−101	−1.2
PCD-007	0.30	0.03	1	0	767	−108	−0.5
NWC-002	0.18	0.01	1	0	740	−109	−0.5
NWC-007	0.26	0.02	1	0	756	−117	−0.8
NWC-008	0.33	0.01	2	2	829	−114	−1.0
NWC-023	0.17	0.01	2	1	872	−97	−0.7
NC-015	0.28	0.02	3	0	792	−109	−0.3
NC-017	0.23	0.01	2	1	829	−91	−0.5
NC-022	0.31	0.03	1	1	754	−109	0.0
NC-039	0.18	0.01	2	2	791	−96	−0.4
Samples from Newman et al. (1988)							
Mc84-T	0.72	0.01	4	0	712	−74	−1.7
Mc84df-Lt	0.66	0.04	4	1	731	n.d.	−1.0
N Coulee	0.23	0.00	2	1	681	−99	−0.8

n.d. not determined

[a] Determined by FTIR

each glass. Minimum detection limits for CO_2 and H_2O_{total} concentrations are 0.6 ppm and 0.04 wt%, respectively, based on uncertainties in glass thickness measurements. Appendix A contains the FTIR data for each point analysis.

Chlorine concentrations were determined using a JEOL JXA-8200 electron microprobe, housed at the University of Texas at Austin. The samples were analyzed with a 40-nA beam current, 15 keV accelerating voltage, and a defocused beam (10 μm diameter). Count times during analysis were On-peak, 90 s; Hi-peak, 60 s; Lo-peak, 60 s. During microprobe sessions a working glass standard (KN18) containing 3,300 ppm Cl was analyzed repeatedly to monitor for analytical quality and instrument drift. The mounted sample sections were analyzed in a series of point analyses (n=3 to 5 per clast; Appendix A), with care taken to avoid vesicles or surface impurities, and averaged for each sample clast and reported in ppm (Table 1). The 1σ error for measured Cl concentration is ±24 ppm, based on numerous measurements of the KN18 glass standard.

Hydrogen and chlorine stable isotopes

Approximately 5 to 10 mg of obsidian material (amount of material used depended on the water content) were extracted from the interior of each clast and crushed into a coarse powder. Care was taken to obtain material from the unaltered core of each clast. These powders were packed into silver capsules and dried under vacuum at 60 °C for at least 48 h. Samples were analyzed for hydrogen isotope compositions using a Thermal Conversion Elemental Analyzer (TC/EA) to produce H_2 gas following the methods of Sharp et al. (2001) and Cassel et al. (2012). The hydrogen gas is then introduced into a ThermoElectronMAT 253 in continuous flow mode to determine the hydrogen isotope composition. δD values are reported in standard per mil notation vs. SMOW (Standard Mean Ocean Water). All samples are calibrated using analyses of internationally distributed hydrogen isotope standards: IAEA C3, IAEA CH7, and NBS-22. An internal volcanic glass standard with a δD value=−145‰ (3.7±0.1 wt.% H_2O) was analyzed to compare inter- and intra-run drift and precision. Replicates of the internal glass standard yielded a standard deviation of ±0.8‰ (1σ). The error for hydrogen isotope composition is dependent on water content. We report errors of ±2‰ for samples with >0.5 wt.% water and ±5‰ for samples with <0.5 wt.% water.

Approximately 120 mg of obsidian material was separated from the center of each clast to avoid surficial alteration and sonicated five times for 15 min each in 18MΩ deionized water to remove any surficial chlorine contamination. Cl^- was released from the powdered, washed obsidian samples by pyrohydrolysis, and collected in an aqueous solution (Magenheim et al. 1994). Once in an aqueous form Cl^- was converted to AgCl and reacted with CH_3I to produce CH_3Cl (Eggenkamp 1994). CH_3Cl was purified on a gas chromatographic column and introduced into a ThermoElectron MAT 253 to determine the chlorine isotope composition (Barnes and Sharp 2006; Sharp et al. 2007). All $\delta^{37}Cl$ values are reported in standard per mil notation versus SMOC (Standard Mean Ocean Chloride). Error for chlorine isotope analysis is ±0.2‰ based on the long-term average of internal seawater standards and an internal serpentinite rock standard.

Results

The H_2O, CO_2, and Cl concentrations, as well as hydrogen and chlorine isotope compositions, of the pyroclastic fall and rhyolitic dome obsidians are summarized in Table 1 (complete data set including replicate analyses are reported in Appendix A). Water concentrations discussed in the results and discussion are based on the H_2O contents determined by FTIR. H_2O contents determined by TC/EA are reported in Appendix A for comparison. Nineteen out of 26 samples from layers P2 and P10, which had replicates for both techniques, were statistically indistinguishable at the 95 % level, indicating there is good agreement between the two techniques for samples with H_2O contents >~0.5 wt.%. For samples with water contents <~0.5 wt.% H_2O, the H_2O contents determined by TC/EA are consistently lower than those determined by FTIR.

For comparison, we analyzed H_2O and CO_2 concentrations and δD values of three samples from the Newman et al. (1988) study: Mc84-T, Mc84df-Lt, and North Coulee. These samples have H_2O concentrations of 0.72, 0.66, and 0.23 wt.%, respectively, and CO_2 concentrations of 4, 4, and 2 ppm, respectively. These values are nearly identical to those reported in Newman et al. (1988): Mc84-T=0.77 wt.% H_2O and 5 ppm CO_2; Mc84df-Lt=0.67 wt.% H_2O and 7 ppm CO_2; and North Coulee=0.27 wt.% H_2O and 2 ppm CO_2. Mc84-T, Mc84df-Lt, and North Coulee have Cl concentrations of 712, 731, and 681 ppm, respectively. Newman et al. (1988) report a δD value of −107‰ for North Coulee, compared to our determined value of −99‰ (almost within 1σ error of one another); and duplicate analyses of −76 and −73‰ for Mc84-T, compared to −74‰ determined here. δD values were not determined for Mc84df-Lt in this study; δD values presented in Figs. 3, 4, and 5 for Mc84df-Lt are from Newman et al. (1988).

H_2O, CO_2, and Cl concentrations

Figure 2 illustrates the range and averages of H_2O and CO_2 concentrations in the horizons P2 and P10 as well as the dome obsidians, including North Coulee from Newman et al. (1988). In general, concentrations of both H_2O and CO_2 decrease from the lower horizon P2 to the upper horizon P10 to the domes. Although the measured water and carbon dioxide concentrations from the two horizons overlap, they represent two distinct populations (Fig. 3a). The H_2O concentrations of the dome obsidians are distinctly lower (with no overlap) than those in either the P2 or P10 horizon. The CO_2 concentrations of the dome obsidians are also distinctly lower

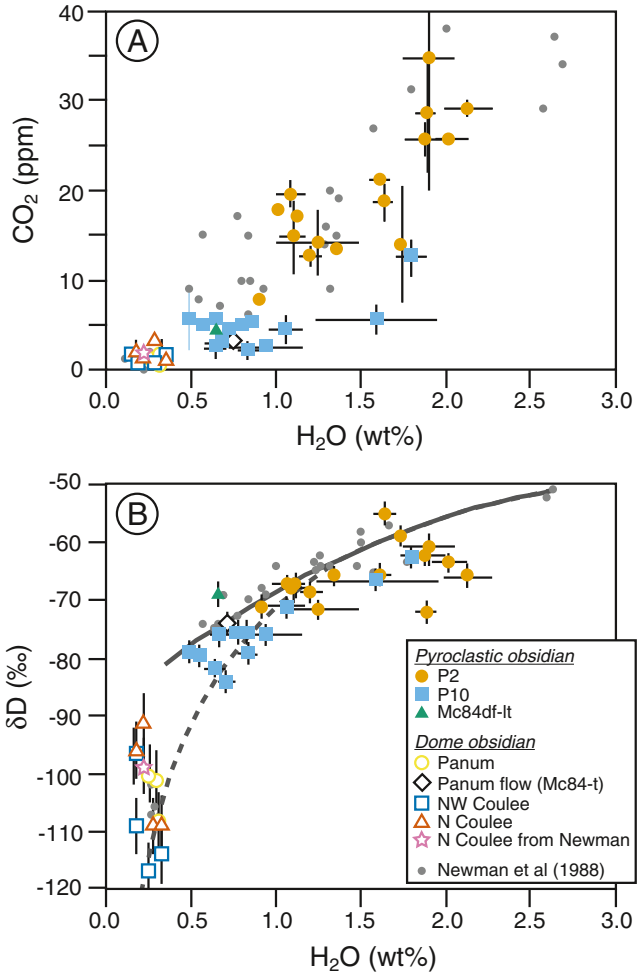

Fig. 3 **a** CO_2 vs. H_2O concentrations of pyroclastic and dome obsidian from Mono Craters. *Large symbols* show data determined in this study. *Small gray circles* show data from Newman et al. (1988) for comparison. **b** δD values vs. H_2O concentrations of pyroclastic and dome obsidian from Mono Craters. *Solid gray line* = closed system degassing model using a varying fractionation factor (α) as a function of water content. *Dashed gray line* = open system degassing model using a varying fractionation factor (α) as a function of water content and continuous loss of vapor from the system

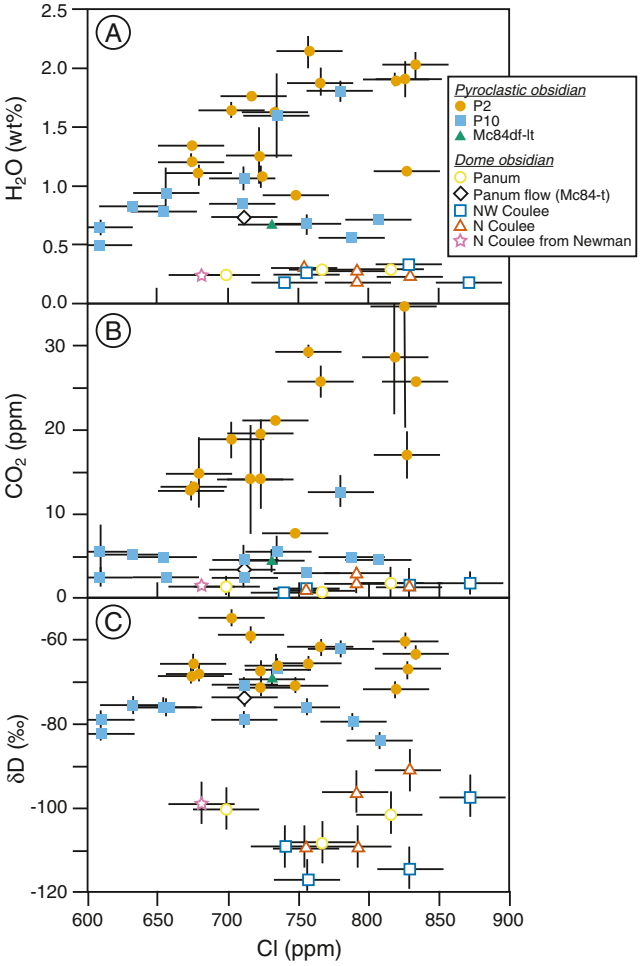

Fig. 4 Variations of Cl concentration versus **a** H_2O concentration, **b** CO_2 concentration, and **c** δD values of pyroclastic and dome obsidian. Same symbols as in Fig. 3

than those in either the P2 or P10 horizon, with slight overlap with the P10 horizon.

In general, the glasses have relatively homogeneous Cl concentrations within an individual clast (Appendix A). But, in contrast to H_2O and CO_2 concentrations, there are no variations in Cl concentration between horizon P2, horizon P10, and the dome samples (Fig. 2). Each group significantly overlaps the others: P2 has an average Cl concentration of 747±57 ppm, P10 averages 704±71 ppm Cl, and the domes average 777±56 ppm Cl (Table 1, Figs. 2 and 4).

Stable isotope compositions

δD values range from −72‰ to −55‰ in the obsidian pyroclasts from layer P2, with an average value of −65±5‰ for the horizon. The δD values range from −84‰ to −62‰ in the obsidian pyroclasts from layer P10, with an average value of −76±6‰ for the horizon. δD values in the lava dome samples range from −117‰ to −91‰. δD values systematically decrease with decreasing H_2O content (Fig. 3b).

$\delta^{37}Cl$ values range from −1.9‰ to −0.1‰ in the obsidian pyroclasts from layer P2, with an average value of −0.8±0.6‰ for the horizon (Fig. 5). The $\delta^{37}Cl$ values range from −1.5‰ to −0.1‰ in the pyroclasts from layer P10, with an average value of −0.8±0.4‰ for the horizon. $\delta^{37}Cl$ values in the obsidian dome samples range from −1.2‰ to 0.0‰, with an average value of −0.6±0.3‰. There are subtle variations among the domes, with North Coulee having the highest $\delta^{37}Cl$ values (−0.8‰ to 0.0‰). Panum and Northwest Coulee have lower, but overlapping $\delta^{37}Cl$ values, ranging from −1.2‰ to −0.5‰ and −1.0‰ to −0.5‰, respectively. There are no correlations between $\delta^{37}Cl$ values and H_2O, CO_2, or Cl concentrations. There is also no correlation between $\delta^{37}Cl$ and δD values (Fig. 5).

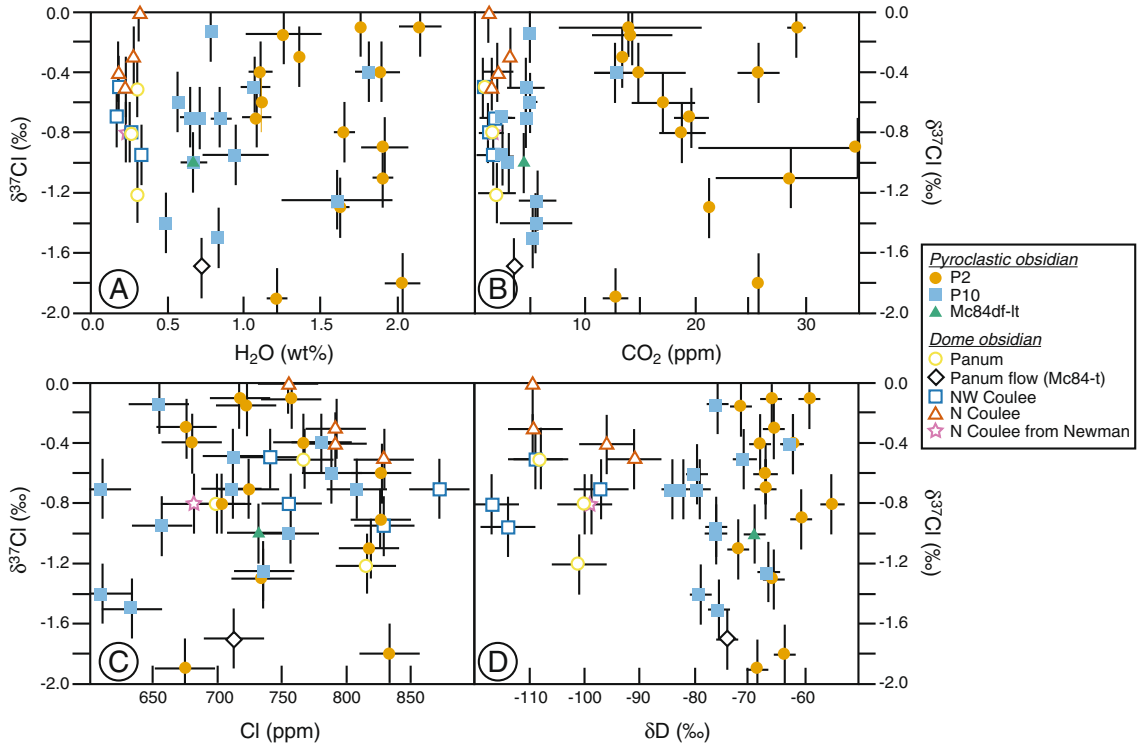

Fig. 5 Chlorine isotope composition of pyroclastic and dome obsidians as a function of **a** H_2O concentration, **b** CO_2 concentration, **c** Cl concentration, and **d** hydrogen isotope composition. Same symbols as in Figs. 4 and 5

Discussion

Open and closed system degassing based on H_2O loss

CO_2 plotted versus H_2O concentration (Fig. 3a) yields a distinctive trend of volcanic degassing in excellent agreement with that observed by Newman et al. (1988). The trend of decreasing δD values with decreasing water content is consistent with a two-stage degassing model (e.g., Taylor et al. 1983; Newman et al. 1988; Taylor 1991). The δD value of the glass (the residual melt) is a function of the partitioning of D and H between melt and co-existing vapor: $\alpha=(D/H)_{vapor}/(D/H)_{melt}$, where α is the isotopic fractionation factor. Hydrogen in the melt is hosted as either molecular H_2O or OH^-, the proportions of which change as a function of total water content and temperature. This degassing trend is modeled using both closed (Batch fractionation, solid gray line in Fig. 3b) and open (Rayleigh fractionation, dashed gray line in Fig. 3b) system degassing with a changing bulk vapor-water fractionation factor, based on the relative proportions of molecular water versus hydroxyl groups (Appendix A), and the fractionation factors of $\alpha_{vapor\text{-}H2O\ molecular}=0.9896$ and $\alpha_{vapor\text{-}OH^-}=1.0415$ (Dobson et al. 1989; Taylor 1991). The models assume a starting water content of 2.64 wt % and a δD value of −51‰, both of which are the highest values reported in the larger Newman et al. (1988) data set. The Rayleigh model is a numerical solution, taking into account the δD value of the exsolved vapor. Consistent with the Newman et al. (1988) study, a closed system model can explain the hydrogen isotope and water content data of the pyroclastic obsidians, but an open system model is necessary to explain the low δD values of the dome glasses (Fig. 3b). This assumes that the pyroclastic obsidians and the dome obsidians are derived from the same isotopically homogeneous parent melt.

Although a closed system degassing model may explain the hydrogen isotope and water concentration relationship of the pyroclastic obsidians, subsequent researchers have argued the model is inconsistent with the high CO_2/H_2O concentration ratios in the Mono Craters obsidians (Rust et al. 2004; Gonnermann and Manga 2005). Newman et al. (1988) proposed 5 wt.% H_2O and 1.2 wt.% CO_2 in the initial melt. Such high CO_2/H_2O concentration ratios require either the presence of a CO_2-rich vapor (Rust et al. 2004), nonequilibrium degassing (Gonnermann and Manga 2005), or a rhyolite melt saturated with a 60 mol.% water fluid that comes from ~1.5 GPa, based on the Liu et al. (2005) model. In the next two sections (the "Behavior of chlorine during volcanic degassing" and the "Sources of chlorine in the Mono Craters system" sections), we use our Cl data to speculate about the role of possible vapor fluxing, buffering by a separate brine phase, or disequilibrium effects due to the slow diffusion of Cl in silicic melts compared to H_2O and CO_2 (Watson 1991; Bai and Koster van Groos 1994; Lowenstern 2000; Baker and Balcone-Boissard 2009) in affecting the Cl chemistry of the Mono Crater obsidians.

Behavior of chlorine during volcanic degassing

The behavior of chlorine during volcanic degassing depends on the solubility of Cl in melt, which is in turn a function of melt composition, fluid composition, temperature, and pressure (e.g., Metrich and Rutherford 1992; Carroll and Webster 1994; Webster et al. 1999; Aiuppa et al. 2009). In general, Cl concentration in the melt decreases or increases depending on whether water is lost (open-system) or not (closed-system), respectively. For example, in the presence of a pure H_2O fluid, Cl solubility in melt increases with decreasing water pressure and decreasing temperature during closed-system degassing (e.g., Carroll and Webster 1994; Gardner et al. 2006). This inverse relationship between solubility and pressure implies that Cl concentration should actually increase during magma decompression (Carroll 2005; Gardner et al. 2006), thereby reducing chloride loss from the residual melt (Aiuppa et al. 2009). This is particularly true in basaltic melt because of the relatively higher Cl solubility in basaltic melt compared to rhyolitic melt (Webster et al. 1999; Chevychelov and Suk 2003). We note that these experimental data are restricted to higher pressures (>50 MPa), in which chloride occurs as alkali chlorides. At lower pressures pressures (~0.1 MPa), HCl is the dominant chloride species (Shinohara 2009). In contrast to the inverse relationship between Cl solubility and pressure for alkali chlorides, HCl solubility decreases with decreasing pressure, allowing Cl to be lost from the melt as HCl at very shallow depths (Iwasaki and Katsura 1967; Shinohara 2009). Experimental data show that during open-system degassing, in which water is allowed to escape from the system, Cl will be lost from the magma as water exsolves, regardless of Cl speciation (Gardner et al. 2006). This occurs because some Cl is partitioned into the H_2O phase, which is subsequently lost. Despite varying chlorine behavior during degassing due to speciation and whether water was lost, chlorine concentrations in the investigated Mono Crater samples remain constant demonstrating no chlorine loss.

In natural samples, matrix glass in volcanic pumice often contains less Cl than was originally dissolved in the magma, as preserved in glass inclusions (e.g., Dunbar et al. 1989; Palais and Sigurdsson 1989; Dunbar and Kyle 1992); therefore, the Cl content of the melt can decrease during magma ascent. However, estimates of volatile loss from volcanic eruptions, based on the pre-eruptive volatile content of melt inclusions in phenocrysts compared to the volatile content in matrix (degassed) glass, show that volatile loss during degassing is largely a function of melt composition (Devine et al. 1984; Palais and Sigurdsson 1989). In general, volatile fluxes from rhyolitic eruptions are one to two orders of magnitude lower than those from basaltic eruptions. For example, the 131 A.D. eruption of Taupo in New Zealand produced 35 km^3 of rhyolite, yet overall a negligible amount of chlorine was lost, despite a lower Cl concentration in matrix glass compared to melt inclusions (Dunbar et al. 1989; Palais and Sigurdsson 1989). Later work on, the 1991 eruption of Mt. Pinatubo also showed minor loss of Cl, despite water loss, during degassing of the melt (Gerlach et al. 1996). Although the 2008–2009 rhyolitic eruption of Volcán Chaitén, Chile, is an exception with Cl loss attributed to degassing of HCl at low pressure and crystallization of microlites (Lowenstern et al. 2012). The case of Volcán Chaitén differs from the one presented here in that the Mono Craters pyroclasts are quenched at higher pressures with minimal microlite crystallization.

Our data show relatively constant chlorine concentrations in both pyroclastic and dome samples, independent of H_2O and CO_2 concentrations and δD values (Fig. 4). The slopes of best fit lines of Cl concentration versus H_2O concentration are not significantly different from zero, indicating no relationship exists between Cl and H_2O concentration (Fig. 4a). The constant Cl concentrations among layer P2, layer P10, and the rhyolitic domes imply that chlorine was not lost throughout the eruptive sequence, despite significant changes in CO_2 and H_2O concentrations. If one excludes the data from the dome samples, then there is a slight trend of decreasing Cl concentration with decreasing CO_2 and H_2O, with many outliers with low H_2O concentrations, but high Cl concentrations (Fig. 4a, b). If we assume that the P2 and P10 layers represent the closed system portion of the eruptive sequence, then the high Cl concentrations may be a function of the decrease in pressure, and hence increasing Cl solubility. But, the presence of numerous samples with high Cl concentrations, despite low H_2O contents, and the large range in Cl concentrations in the dome obsidians argue against significant Cl loss during degassing. These observations are consistent with above experimental and empirical data for limited Cl loss during degassing, particularly in rhyolitic systems.

We note that the relatively constant Cl concentrations in the obsidians do not necessitate negligible Cl degassing (e.g., Shinohara 2009). Because halogens are highly incompatible, the Cl concentration in the melt is a function of both the crystallization of the melt and volcanic degassing (Villemant and Boudon 1999; Villemant et al. 2003, 2008). However, as we show below, crystallization cannot account for the observed Cl concentrations in our samples. In contrast to our study, other studies observe a decrease in Cl concentration with decreasing H_2O concentration from mineral-hosted melt inclusions to pyroclastic air-fall clasts to dome fragments (e.g., 650 year b.p. eruption at Mt. Pelée, Martinique; Santa Maria, Guatemala; Taupo volcanic center, New Zealand; Soufrière Hills, Montserrat; Obsidian Dome, Inyo Domes; Westrich et al. 1988; Dunbar et al. 1989; Dunbar and Kyle 1992; Villemant and Boudon 1998, 1999; Villemant et al. 2003, 2008). All of these eruptions require an open system degassing model to fit the low Cl concentration data (Dunbar and Kyle 1992; Villemant et al. 2003). However, Villemant et al. (2003) argue that the open system model

requires crystallization of the melt for the best fit. For example, the pyroclastic fall and dome obsidians from the Mt. Pelée eruption have ~16–30 wt.% microlites in the groundmass, demonstrating that the melt partially crystallized (Villemant et al. 2003). In contrast, the pyroclastic obsidians from our study are essentially holohyaline (P2<< 0.1 % microlites and P10≈0.5 % microlites) and the dome obsidians are only slightly more crystallized (~2–5 %; see the "Geologic setting and sampling" section). All have similar Cl concentrations (Fig. 2). The microlite phases are anhydrous (oxide minerals, feldspar, pyroxene); i.e., not minerals that typically host large amounts of Cl, like amphibole and biotite. If we take an extreme case, and assume 5 % crystallization of microlites devoid of Cl, then microlite crystallization could only account for a ~35 ppm increase in Cl concentration in the melt starting from 600 ppm. This change is far less than the overall Cl variation observed in the obsidians (Figs. 2 and 4). A lower microlite content and/or a higher Cl concentration in the microlite phases will result in an even lower change in the Cl concentration of the melt. In addition, the higher microlite content in the domes, compared to the pyroclastic obsidians, would predict that the domes should be more enriched in Cl, but this is not observed. The lack of microlites in the P2 and P10 layers, the constant Cl concentration despite the variation in microlite density between the pyroclastic and dome obsidians, and the lack of Cl-hosting anhydrous phases argue against crystallization as a potential counter balance to Cl degassing.

Alternatively, three possible explanations exist for the constant Cl concentration: (a) Cl fluxing, (b) buffering by a separate brine phase, and (c) disequilibrium degassing. The first possible explanation is continual fluxing of a Cl-rich vapor from a deeper magmatic source. Similar arguments of CO_2 fluxing to shallow magmas are a common explanation for CO_2/H_2O ratios in melt inclusions and obsidians too high to be explained by volcanic degassing (e.g., Anderson et al. 1989; Rust et al. 2004; Roberge et al. 2009; Blundy et al. 2010; Johnson et al. 2010; Yoshimura and Nakamura 2011). Teleseismic data document the presence of a low-velocity anomaly, with a melt fraction of ~20 %, at ~8–10 km depth beneath Mono Craters (Achauer et al. 1986). This anomaly has been interpreted as a magma chamber (Achauer et al. 1986) or a plutonic crystal mush (Hildreth 2004). Dike sources from this body feed the Mono Crater domes, with possible stagnation in melt lenses in between (Bursik 1993; Hildreth 2004). Cl fluxing from this magma chamber could have buffered the Cl concentration in the Mono Crater obsidians. This may be evident in the pyroclastic and dome obsidians with low water contents, yet high Cl concentrations. However, as suggested above, these high Cl concentrations may simply be a function of decreasing pressure, and hence increasing Cl solubility.

Secondly, interaction with a separate brine phase has the potential to buffer the Cl concentration of the melt. Lowenstern (2000) argues that in many mid- to upper-crustal reservoirs, the Cl concentration in silicate melt may be buffered by the presence of a brine. The presence of this brine results from the non-ideal behavior of alkali chlorides unmixing to produce a H_2O-rich vapor and a hydrosaline phase at high pressures (Lowenstern 2000). The Cl concentration in a "buffered" melt is a function of the composition of the melt (Webster 1997; Lowenstern 2000). In a rhyolitic melt, the Cl concentration limit is ~2,700 ppm (Metrich and Rutherford 1992). The Cl concentration in the Mono Crater glasses is significantly lower, 742±65 ppm Cl. The Cl concentration in the Mono Crater glasses is thus likely too low for interaction with a brine phase to be a reasonable explanation for the near constant Cl concentration.

Alternatively, the constant Cl concentration, independent of H_2O or CO_2 concentrations and hydrogen isotope composition, may be a kinetic effect, resulting from the relatively slower diffusion of Cl in silicic melt compared to H_2O and CO_2 (Watson 1991; Bai and Koster van Groos 1994; Baker and Balcone-Boissard 2009). Watson (1991) determined bulk diffusivity of dissolved CO_2 and Cl in obsidian melts (76.4 wt.% SiO_2). In a melt with 8 wt.% water, D_{Cl} is about 5 to 10 times slower than D_{CO2} (Watson 1991). Subsequent Cl diffusion experiments in haplogranitic melt (74.6 wt.% SiO_2) and obsidian melt (77.9 wt.% SiO_2), with varying water contents from 0 to 7 wt.%, support much slower (5 to 8 times lower) diffusivity of chlorine compared to CO_2 (Bai and Koster van Groos 1994). Other studies on the Mono Craters 1340 A.D. eruption argue for nonequilibrium degassing (Gonnermann and Manga 2005; Watkins et al. 2012), in which the slower diffusing CO_2 remains relatively enriched in the melt compared to H_2O, consistent with our observations of Cl behavior. Slow diffusion of Cl has also been used in support of limited Cl degassing during large volcanic eruptions, such as the 1991 eruption of Mt. Pinatubo (Gerlach et al. 1996).

The chlorine isotope data display a wide range of values (from −1.9‰ to 0.0‰), but do not display systematic variation with any of the other measured variables (H_2O, CO_2, or Cl concentration, δD values; Fig. 5). For example, slopes of best fit lines between Cl concentration and H_2O concentration (Fig. 5a) and Cl concentration and $\delta^{37}Cl$ value (Fig. 5c) are not significantly different from zero, implying no significant relationship between the two variables. The lack of correlations between $\delta^{37}Cl$ values and H_2O concentration, CO_2 concentration, or δD values indicate the absence of a systematic fractionation of chlorine stable isotopes during volcanic degassing of CO_2 or H_2O. However, the relatively constant Cl concentration makes it impossible to assess if Cl isotopes fractionate due to Cl loss.

Sources of chlorine in the Mono Craters system

The $\delta^{37}Cl$ values of both the pyroclastic and dome obsidians have a remarkably large range of almost 2‰ (compared to the

~6‰ range documented in volcanic outputs (ash, tephra, lava) globally (Barnes et al. 2008, 2009; Barnes and Straub 2010; Rizzo et al. 2013)). In addition, there is up to 0.7‰ variability for a given dome. Based on the data presented here, this large variability is unlikely the result of fractionation effects due to volcanic degassing. A possible mechanism to explain the isotopic variability is fractionation between melt and silicate mineral phases, such as hornblende, biotite and apatite. Based on theoretical calculations, ^{37}Cl will be preferentially enriched in minerals in which Cl is bonded to +2 cations (e.g., amphibole, biotite; Schauble et al. 2003). This is consistent with empirical work on altered oceanic crust, in which positive δ^{37}Cl values are recorded in amphibole-rich sections of altered oceanic crust (Barnes and Cisneros 2012). After precipitation of hornblende, biotite, and/or apatite, the remaining melt will be depleted in ^{37}Cl. Calculations of equilibrium stable Cl isotope fractionation predict that a silicate mineral should have higher δ^{37}Cl values (~2‰ to 3‰ higher at room temperature) than coexisting brine (Schauble et al. 2003). Extrapolations to higher temperatures show the fractionation decreases to ~0.2 ‰ higher in the silicate mineral at ~800 °C. If one assumes that 90 % of the original Cl in the system is removed by crystallization, then the maximum variation in the δ^{37}Cl value is ~0.5‰. In addition, there is a near absence of Cl-bearing phenocrysts in the Mono Craters melt. Therefore, the diversity in δ^{37}Cl values cannot be a result of crystallization.

Instead, the variability of the chlorine isotopic compositions in the obsidian samples likely indicates heterogeneity in parental magmas. The upper mantle has a relatively consistent δ^{37}Cl value of −0.2±0.3‰ (Sharp et al. 2007, 2013), although some variability has been documented resulting from to the subduction of crustally derived material (Sharp et al. 2007; John et al. 2010). Based on the relatively constant δ^{37}Cl value of the upper mantle, the range of δ^{37}Cl values in these glasses is noteworthy, particularly given the variability within an individual dome (up to 0.7‰). The variability in the δ^{37}Cl value of the pyroclastic fall obsidians and domes may reflect some variability in the initial upper mantle composition (e.g., −0.5‰ to 0.0‰) with subsequent isotopic modification due to assimilation of crustal material. Sedimentary material has a distinctly negative δ^{37}Cl value ranging from −2.6‰ to +0.7 ‰ (n=48) with most samples having values between ~−2‰ and 0‰ (Arcuri and Brimhall 2003; Barnes et al. 2008, 2009). Assimilation of isotopically negative sedimentary material to an originally negative mantle melt can explain values as low as the −1.9‰ documented at Mono Craters. It is also interesting to note that the 1340 A.D. eruption began at North Coulee and migrated northwards (Wood 1983; Sieh and Bursik 1986) and North Coulee has the most mantle-like δ^{37}Cl value (−0.3±0.2‰) of the three domes analyzed. The later erupted domes (Northwest Coulee and Panum Crater) have lower δ^{37}Cl values, consistent with subsequent assimilation of sedimentary material. However, one would expect to find a correlation of Cl concentration with δ^{37}Cl value if assimilation of Cl-bearing sediments were responsible for the low δ^{37}Cl values. No such trend is documented. Minor and trace elemental (Mn, Mg, Ti, K, Cl, P) concentrations in samples that span the complete range of δ^{37}Cl values are homogeneous, and do not vary with the wide range of δ^{37}Cl values (Appendix B). This is consistent with Newman et al. (1988), who also noted the absence of variation in major and minor element chemistry other than volatiles in the Mono Craters obsidians. These data imply minimal assimilation of crustal material or mixing of different magmatic end-members.

Finally, the chlorine isotope variability may be due to a shallow crustal melt/mush, with an initial δ^{37}Cl value of ~−1.5‰, which has been fluxed with varying amounts of mantle-derived chlorine. Variable amounts of Cl fluxing could explain the variable Cl isotope compositions recorded in the Mono Crater obsidians, yet relatively constant Cl concentration. However, mass balance constraints argue that to change the isotopic composition of a crustal end-member (~−1.5‰) to that of a near mantle end-member (~ 0‰) would require that most of the Cl is sourced from a deeper mafic melt.

Conclusions

Chlorine stable isotopes are independent of H_2O and CO_2 concentration and δD values, supporting the use of chlorine as a conservative tracer of fluid source in various geologic settings despite possible H_2O and CO_2 loss. However, additional work is needed to determine if Cl isotopes fractionate in response to significant Cl loss during volcanic degassing. The large variability in the chlorine isotope composition of the volcanic glasses may reflect modification of a melt partially contaminated by sedimentary material or a crustal melt modified by varying amounts of Cl fluxing from a deeper mafic melt. Fluxing of Cl may also explain the buffering of Cl concentrations to a relatively constant value.

Cl concentrations in pyroclastic fall and dome obsidians are also independent of H_2O and CO_2 concentration and δD and δ^{37}Cl values. The constant Cl concentration despite H_2O and CO_2 loss may be a kinetic effect due to the relatively slow diffusion of Cl. These observations are consistent with other studies suggesting nonequilibrium degassing at Mono Craters (Gonnermann and Manga 2005; Watkins et al. 2012).

Acknowledgments The authors gratefully acknowledge S. Newman for providing three obsidian samples from her prior study, B. Andrews and R. Zinke for help in the field, D. Breecker for help with statistics, and H. Gonnermann for helpful discussions. The authors thank J. Watkins and J. Lowenstern for helpful and prompt reviews, as well as, M. Manga for editorial handling and thoughtful comments. This work represents T. Prather's undergraduate honors thesis and was supported by NSF-EAR-0946686 to J.D.B. and J.E.G.

References

Achauer U, Greene L, Evans JR, Iyer HM (1986) Nature of the magma chamber underlying the Mono Craters area, Eastern California, as determined from teleseismic travel time residuals. J Geophys Res 91:13873–13891

Aiuppa A, Baker DR, Webster JD (2009) Halogens in volcanic systems. Chem Geol 263:1–18

Anderson AT, Newman S, Williams SN, Druitt TH, Skirius C, Stolper E (1989) H2O, C02, CI, and gas in Plinian and ash-flow Bishop rhyolite. Geology 17:221–225

Arcuri T, Brimhall G (2003) The chloride source for atacamite mineralization at the Radomiro Tomic porphyry copper deposit, northern Chile. Econ Geol 98:1667–1681

Bai TB, Koster van Groos AF (1994) Diffusion of chlorine in granitic melts. Geochim Cosmochim Acta 58:113–123

Baker DR, Balcone-Boissard H (2009) Halogen diffusion in magmatic systems: our current state of knowledge. Chem Geol 263:82–88

Barnes JD, Cisneros M (2012) Mineralogical control on the chlorine isotope composition of altered oceanic crust. Chem Geol 326–327:51–60

Barnes JD, Sharp ZD (2006) A chlorine isotope study of DSDP/ODP serpentinized ultramafic rocks: insights into the serpentinization process. Chem Geol 228:246–265

Barnes JD, Sharp ZD, Fischer TP (2008) Chlorine isotope variations across the Izu-Bonin-Mariana arc. Geology 36:883–886

Barnes JD, Sharp ZD, Fischer TP, Hilton DR, Carr MJ (2009) Chlorine isotope variations along the Central American volcanic front and back arc. Geochem Geophys Geosyst 10, Q11S17, doi:10.1029/2009GC002587

Barnes JD, Straub SM (2010) Chlorine stable isotope variations in Izu Bonin tephra: implications for serpentinite subduction. Chem Geol 272:62–74

Befus KS, Gardner JE, Zinke RW (2012) Analyzing water contents in unexposed glass inclusions in quartz crystals. Am Mineral 97:1898–1904

Behrens H, Schmidt MO (1998) Infrared spectroscopy of hydrous silicic glasses at temperatures up to 600 °C and implications for the incorporation and dynamics of water in glasses. N Jb Mineral 172: 203–226

Behrens H, Tamic N, Holtz F (2004) Determination of the molar absorption coefficient for the infrared absorption band of CO2 in rhyolitic glasses. Am Mineral 89:301–306

Blundy J, Cashman KV, Rust A, Witham F (2010) A case for CO_2-rich arc magmas. Earth Planet Sci Lett 290:289–301

Bursik M (1993) Subplinian eruption mechanisms inferred from volatile and clast disperal data. J Volcanol Geotherm Res 57:57–70

Bursik M, Sieh K (1989) Range front faulting and volcanism in the Mono Basin, Eastern California. J Geophys Res 94:15587–15609

Carroll MR (2005) Chlorine solubility in evolved alkaline magmas. Ann Geophys 48:619–631

Carroll MR, Webster JD (1994) Solubilities of sulfur, noble gases, nitrogen, chlorine, and fluorine in magmas. In: Carroll MR, Holloway JR (eds) Volatiles in Magmas, Rev. Mineral., pp 231–279

Cassel EJ, Graham SA, Chamberlain C, Henry CD (2012) Early Cenozoic topography, morphology, and tectonics of the northern Sierra Nevada and western Basin and Range. Geosphere 8:229–249

Chevychelov VY, Suk NI (2003) Influence of the composition of magmatic melt on the solubility of metal chlorides at pressures of 0.1-3.0 kbar. Petrology 11:62–74

Devine JD, Sigurdsson H, Davis AN, Self S (1984) Estimates of sulfur and chlorine yield to the atmosphere from volcanic eruptions and potential climatic effects. J Geophys Res 89(B7):6309–6325

Dobson PF, Epstein S, Stolper EM (1989) Hydrogen isotope fractionation between co-existing vapor and silicate glasses and melts at low pressure. Geochim Cosmochim Acta 53:2723–2730

Dunbar NW, Hervig RL, Kyle PR (1989) Determination of pre-eruptive H_2O, F, and Cl contents of silicic magmas using melt inclusions: examples from Taupo volcanic center, New Zealand. Bull Volcanol 51:177–184

Dunbar NW, Kyle PR (1992) Volatile contents of obsidian clasts in tephra from the Taupo Volcanic Zone, New Zealand: Implications to eruptive processes. J Volcanol Geotherm Res 49:127–145

Eggenkamp HGM (1994) The geochemistry of chlorine isotopes. Ph.D. thesis. Uniersiteit Utrecht. p 151

Gardner JE, Burgisser A, Hort M, Rutherford M (2006) Experimental and model constraints on degassing of magma during ascent and eruption. In: Siebe C, Macías JL, Aguirre-Díaz GJ (eds) Neogene-Quaternary continental margin volcanism: A perspective from Mexico. Geological Society of America Special Paper 402, Penrose Conference Series, pp 99–113

Gerlach TM, Westrich HR, Symonds RB (1996) Preeruption vapor in magma of the climactic Mount Pinatubo eruption: source of the giant stratospheric sulfur dioxide cloud. In: Newhall CG, Punongbayan RS (eds) Fire and mud: eruptions and Lahars of Mount Pinatubo, Philippines. University of Washington Press, Seattle, pp 415–433

Gonnermann HM, Manga M (2005) Nonequilibrium magma degassing: results from modeling of the ca. 1340 A.D. eruption of Mono Craters, California. Earth Planet Sci Lett 238:1–16

Higgins MD, Meilleur D (2009) Development and emplacement of the Inyo Domes magmatic suite, California: evidence from geological, textural (CSD) and geochemical observations of ash and lava. J Volcanol Geotherm Res 186:280–292

Hildreth W (2004) Volcanological perspectives on Long Valley, Mammoth Mountain, and Mono Craters: several contiguous but discrete systems. J Volcanol Geotherm Res 136:169–198

Ihinger PD, Hervig RL, McMillan PF (1994) Analytical methods for volatiles in glasses. In: Carroll MR, Holloway JR (eds) Volatiles in Magmas. Reviews in Mineralogy. Mineralogical Society of America, Washington D.C., pp 67–121

Iwasaki B, Katsura T (1967) The solubility of hydrogen chloride in volcanic rock melts at a total pressure of one atmosphere and at temperatures of 1,200 °C and 1,290 °C under anhydrous conditions. Bull Chem Soc Jpn 40:554–561

John T, Layne GD, Haase KM, Barnes JD (2010) Chlorine isotope evidence for crustal recycling into the Earth's mantle. Earth Planet Sci Lett 298:175–182

Johnson ER, Wallace PJ, Cashman KV, Delgado Granados HD (2010) Degassing of volatiles (H_2O, CO_2, S, Cl) during ascent, crystallization, and eruption at mafic monogenetic volcanoes in central Mexico. J Volcanol Geotherm Res 197:225–238

Kelleher PC, Cameron KL (1990) The geochemistry of the Mono Craters-Mono Lake Islands volcanic complex, eastern California. J Geophys Res 95:17643–17659

Leschik M, Heide G, Frischat GH, Behrens H, Wiedenbeck M, Wagner N, Heide K, Beibler H, Reinholz U (2004) Determinination of H2O and D2O contents in rhyolitic glasses. Phys Chem Glas—Eur J Glas Sci Technol B 45:238–251

Liebscher A, Barnes JD, Sharp ZD (2006) Chlorine isotope vapor-liquid fractionation during experimental fluid-phase separation at 400 °C/23 MPa to 450 °C/42 MPa. Chem Geol 234:340–345

Liu Y, Zhang Y, Behrens H (2005) Solubility of H_2O in rhyolitic melts at low pressures and a new empirical model for mixed H_2O-CO_2 solubility in rhyolitic mels. J Volcanol Geotherm Res 143:219–235

Lowenstern JB (2000) A review of the contrasting behavior of two magmatic volatiles: chlorine and carbon dioxide. J Geochem Explor 69:287–290

Lowenstern JB, Bleick H, Vazquez JA, Castro JM, Larson PB (2012) Degassing of Cl, F, Li, and Be during extrusion and crystallization of the rhyolitic dome at Volcán Chaitén, Chile during 2008 and 2009. Bull Volcanol 74:2303–2319

Magenheim AJ, Spivack AJ, Volpe C, Ransom B (1994) Precise determination of stable chlorine isotopic ratios in low-concentration natural samples. Geochim Cosmochim Acta 58(14):3117–3121

Metrich N, Rutherford MJ (1992) Experimental study of chlorine behavior in hydrous silicic melts. Geochim Cosmochim Acta 56:607–616

Newman S, Epstein S, Stolper E (1988) Water, carbon dioxide, and hydrogen isotopes in glasses from the ca. 1340 A.D. eruption of the Mono Craters, California: constraints on degassing phenomena and initial volatile content. J Volcanol Geotherm Res 35:75–96

Newman S, Stolper EM, Epstein S (1986) Measurement of water in rhyolitic glasses: calibration of an infrared spectroscopic technique. Am Mineral 71:1527–1541

Okumura S, Nakamura M, Nakashima S (2003) Determination of molar absorptivity of IR fundamental OH-stretching vibration in rhyolitic glasses. Am Mineral 88:1657–1662

Palais JM, Sigurdsson H (1989) Petrologic evidence of volatile emissions from major historic and pre-historic volcanic eruptions. In: Understanding Climate Change, Geophys. Monogr. Ser 52 pp 31–53

Rizzo AL, Caracausi A, Liotta M, Paonita A, Barnes JD, Corsaro RA, Martelli M (2013) Chlorine isotopic composition of volcanic gases and rocks at Mount Etna (Italy) and inferences on the local mantle source. Earth Planet Sci Lett 371:134–142

Roberge J, Delgado Granados H, Wallace PJ (2009) Mafic magma recharge supplies high CO_2 and SO_2 gas fluxes from Popocatépetl volcano, Mexico. Geology 37:107–110

Rust AC, Cashman KV, Wallace PJ (2004) Magma degassing buffered by vapor flow through brecciated condiut margins. Geology 32: 349–352

Schauble EA, Rossman GR, Taylor HPJ (2003) Theoretical estimates of equilibrium chlorine-isotope fractionations. Geochim Cosmochim Acta 67(17):3267–3281

Sharp ZD, Atudorei V, Durakiewicz T (2001) A rapid method for determination of hydrogen and oxygen isotope ratios from water and solid hydrous substances. Chem Geol 178:197–210

Sharp ZD, Barnes JD, Brearley AJ, Chaussidon M, Fischer TP, Kamenetsky VS (2007) Chlorine isotope homogeneity of the mantle, crust and carbonaceous chondrites. Nature 446:1062–1065

Sharp ZD, Barnes JD, Fischer TP, Halick M (2010) A laboratory determination of chlorine isotope fractionation in acid systems and applications to volcanic fumaroles. Geochim Cosmochim Acta 74: 264–273

Sharp ZD, Mercer JA, Jones RH, Brearley AJ, Selverstone J, Bekker A, Stachel T (2013) The chlorine isotope composition of chondrites and Earth. Geochim Cosmochim Acta 107:189–204

Shinohara H (2009) A missing link between volcanic degassing and experimental studies on chloride partitioning. Chem Geol 263: 51–59

Sieh K, Bursik M (1986) Most recent eruption of the Mono Craters, eastern central California. J Geophys Res 91:12539–12571

Taylor BE (1991) Degassing of Obsidian Dome rhyolite, Inyo volcanic chain, California. In: Taylor HP, O'Neil JR, Kaplan IR (eds) Stable Isotope Geochemistry: A Tribute to Samuel Epstein. The Geochemical Society, Special Publication, pp 339–353

Taylor BE, Eichelberger JC, Westrich HR (1983) Hydrogen isotopic evidence of rhyolitic magma degassing during shallow intrusion and eruption. Nature 306:541–545

Villemant B, Boudon G (1998) Transition from dome-forming to plinian eruptive styles controlled by H_2O and Cl degassing. Nature 392:65–69

Villemant B, Boudon G (1999) H_2O and halogen (F, Cl, Br) behaviour during shallow magma degassing processes. Earth Planet Sci Lett 168:271–286

Villemant B, Boudon G, Nougrigat S, Potreaux S, Michel A (2003) Water and halogens in volcanic clasts: tracers of degassing processes during Plinian and dome-building eruptions. In: Oppenheimer C, Pyle DM, Barclay J (eds) Volcanic Degassing. Geol. Soc. London Spec. Publ., pp 63–79

Villemant B, Mouatt J, Michel A (2008) Andesitic magma degassing investigated through H2O vapour-melt partitioning of halogens at Soufrière Hills Volcano, Montserrat (Lesser Antilles). Earth Planet Sci Lett 269:212–229

Watkins J, DePaolo D, Ryerson F, Peterson B (2011) Influence of liquid structure on diffusive isotope separation in molten silicates and aqueous solutions. Geochim Cosmochim Acta 75:3103–3118

Watkins JM, Manga M, DePaolo DJ (2012) Bubble geobarometry: a record of pressure changes, degassing, and regassing at Mono Craters, California. Geology 40:699–702

Watson EB (1991) Diffusion of dissolved CO2 and Cl in hydrous silicic to intermediate magmas. Geochim Cosmochim Acta 55:1897–1902

Webster JD (1997) Chloride solubility in felsic melts and the role of chloride in magmatic degassing. J Petrol 38:1793–1807

Webster JD, Kinzler RJ, Mathez EA (1999) Chloride and water solubilitiy in basalt and andesite melts and implications for magma degassing. Geochim Cosmochim Acta 63:729–738

Westrich HR, Stockman HW, Eichelberger JC (1988) Degassing of rhyolitic magma during ascent and emplacement. J Geophys Res 93:6503–6511

Wood SH (1983) Chronology of Late Pleistocene and Holocene Volcanics, Long Valley and Mono Basin Geothermal Area, Eastern California. U. S. Geological Survey Open File Report 83–747

Yoshimura S, Nakamura M (2011) Carbon dioxide transport in crustal magmatic systems. Earth Planet Sci Lett 307:470–478

Zhang Y, Belcher R, Ihinger PD, Wan L, Xu Z, Newman S (1997) New calibration of infrared measurement of dissolved water in rhyolitic glasses. Geochim Cosmochim Acta 61:3089–3100